

Annual Review of Biophysics

Mechanisms of Sensory Discrimination: Insights from *Drosophila* Olfaction

Lukas N. Groschner and Gero Miesenböck

Centre for Neural Circuits and Behavior, University of Oxford, Oxford OX1 3SR,
United Kingdom; email: gero.miesenboeck@cncb.ox.ac.uk

**ANNUAL
REVIEWS CONNECT**

www.annualreviews.org

- Download figures
- Navigate cited references
- Keyword search
- Explore related articles
- Share via email or social media

Annu. Rev. Biophys. 2019. 48:209–29

First published as a Review in Advance on
February 20, 2019

The *Annual Review of Biophysics* is online at
biophys.annualreviews.org

<https://doi.org/10.1146/annurev-biophys-052118-115655>

Copyright © 2019 by Annual Reviews.
All rights reserved

Keywords

decision making, neural coding, signal detection, synapse, dendrite, inhibition

Abstract

All an animal can do to infer the state of its environment is to observe the sensory-evoked activity of its own neurons. These inferences about the presence, quality, or similarity of objects are probabilistic and inform behavioral decisions that are often made in close to real time. Neural systems employ several strategies to facilitate sensory discrimination: Biophysical mechanisms separate the neuronal response distributions in coding space, compress their variances, and combine information from sequential observations. We review how these strategies are implemented in the olfactory system of the fruit fly. The emerging principles of odor discrimination likely apply to other neural circuits of similar architecture.

Contents

INTRODUCTION	210
THE ENCODER STAGE	211
Receptors and Communication Channels	211
Adaptation	213
Combinatorial Odor Encoding	213
Gain Control and High-Pass Filtering	216
Stochastic Resonance	217
THE DECODER STAGE	218
Two Systems	218
Expansion Recoding and Sparsening	219
Sequential Sampling	220
Neuronal Noise and Behavioral Variability	223

INTRODUCTION

Neural systems represent information in time-varying combinatorial activity; like voices in a choir, different neurons are electrically active or silent at different times. The two main problems of representation in this, as in any, communication system are how to encode the source data so that their representations are (a) “far apart in some suitable sense” and (b) “minimal for purposes of efficiency” (56, p. 2). Here, we consider the first of these problems in the context of olfaction. We review how a source alphabet of odorous chemicals is converted into a code alphabet of bioelectric signals, explore perceptual limits that can arise from this encoding, and reveal biophysical mechanisms that extend these limits. We do not touch on the problem of how to represent information efficiently, itself a vast and important topic in neuroscience (4, 127).

Because neurons are inherently noisy and repeated presentations of the same stimulus produce different responses even under identical conditions, the relationship between sensory stimuli and neuronal responses is probabilistic: Associated with every stimulus S is a conditional probability distribution of possible responses R , the encoding dictionary $P(R|S)$. The mutual information between S and R provides a global description of this dictionary (8, 28, 56, 115). It quantifies how telling, on average, neural responses are about stimuli and places a bound on the maximal number of stimuli that can be discriminated by observing these responses. The mutual information is zero if responses reveal nothing about stimuli and maximal (and equal to the stimulus entropy) if each stimulus produces a uniquely discernible response. In more technical terms, the mutual information measures the reduction in uncertainty gained by knowing the joint instead of the marginal probability distributions of stimuli and responses (8, 28, 56, 115). This information gain is known as the relative entropy, discrimination information, or Kullback-Leibler divergence from statistical independence (28, 81, 126). The mutual information is large if responses and stimuli are highly correlated.

Although analyses of perceptual decisions and the neural codes underpinning them are often framed in terms of the underlying probability distributions, the moment-by-moment actions of a decision maker must be based on information obtained from individual samples rather than from knowledge of the full distributions (9, 47, 50, 115). The Kullback-Leibler divergence also plays an important role in this situation because it quantifies the ease with which distributions can be discriminated from each other based on samples (8, 28, 126). Imagine that we are shown a series

Stimulus–conditional response distribution (also known as the likelihood function): relative likelihood of different neuronal responses given a stimulus

Mutual information: amount of information one random variable (the neuronal response) contains about another (the stimulus)

Entropy: amount of information contained in a stimulus or response set with known probability distribution

Kullback-Leibler divergence [of $P(R|A)$ from $P(R|B)$]: average information that a single neuronal response to stimulus A provides against B

of neuronal responses R_n and have to determine which of two stimuli, A or B , evoked them. [In other words, we have to compare the likelihood that the responses have come from the encoding dictionaries $P(R|A)$ or $P(R|B)$.] Without rehashing formal arguments found elsewhere (8, 28, 126), we note that the corresponding log likelihood ratio grows linearly with the number of samples n and thus describes a process of accumulating evidence in favor of A over B .

The asymptotic rate of evidence accumulation is the Kullback-Leibler divergence of $P(R|A)$ from $P(R|B)$ (8, 126). For the special case of two Gaussian distributions with different means and identical variances, the divergence is proportional to the square of their discriminability, which is the distance between the means in units of the common standard deviation. Discrimination is thus aided by mechanisms that move the stimulus–conditional response distributions apart from one another, tighten their variances, or enable repetitive sampling. We illustrate these mechanisms in the olfactory system of *Drosophila*, where relative numerical simplicity (130), a well-defined front end (54, 55), a growing understanding of deeper synaptic layers (2, 41, 67, 150), genetic access to many of the relevant circuit elements, and an ability to control these elements during odor discrimination (25, 86, 96) have aligned to make mechanistic ideas precise and testable. Although we rely on particulars of the sensory modality and the organism to ground these ideas in biological reality, we hope to expose general principles and highlight parallels to—or differences from—other systems where limitations in space or our knowledge allow. We occasionally refer to studies in other insects and generally do not differentiate between odor identity and intensity discrimination, recognizing that they are based on representations in a common code (54, 102, 131, 142).

Perhaps the most striking parallel is how closely the architecture of the olfactory system resembles that of other neural structures, especially the cerebellum and the hippocampus (23, 25, 38, 87, 88, 128, 133). In all these systems, sensory information is first encoded in a dense, high-capacity format approximating a maximum-entropy code. This compact representation is then decoded by expansion and sparsening. In all systems, the decoder's discriminatory power is also used as an addressing system for associative memory: Each neuron is an address decoder for a discrete data storage location (25, 73).

THE ENCODER STAGE

Receptors and Communication Channels

Olfactory discrimination in *Drosophila* begins with the interaction of airborne odorants with ~50 functional receptors (26, 44, 140) arrayed across ~50 different types of olfactory receptor neurons (ORNs) (27, 40) (**Figure 1a,b**). Volatile chemicals, aided by odorant-binding proteins (112), partition into the liquid lymph surrounding the ORN dendrites and bind to odorant receptors. In contrast with their mammalian counterparts, which appear exclusively G protein–coupled (14), insect odorant receptors are remarkably diverse: Whereas some odorant receptors may signal via cyclic nucleotides (144), most behave like nonselective cation channels (17, 120, 144); some even share homology with ionotropic glutamate receptors, which hints at an ancestral relationship (6). With no need for second messengers, signal transduction can be fast, with response latencies of <2 ms after odor contact with the surface of the antenna (135), provided there are no solubilization and/or diffusion delays (100, 121).

An individual ORN typically expresses only a single functional odorant receptor (27, 40, 141), which defines the neuron's response spectrum (33, 55) and coassembles with the obligatory coreceptor Orco (83) into a heterotetrameric channel (17). Many odorant receptors are broadly tuned and bind multiple, not always structurally similar odorants with different affinities in a concentration-dependent manner (54, 55); others are highly selective, often for social odors, such as pheromones (82) or the stress odorant CO₂ (134); still others fall on a continuum between

(Log) likelihood ratio: (logarithm of the) ratio of probabilities that a response was produced by stimulus A or B

ORN: olfactory receptor neuron

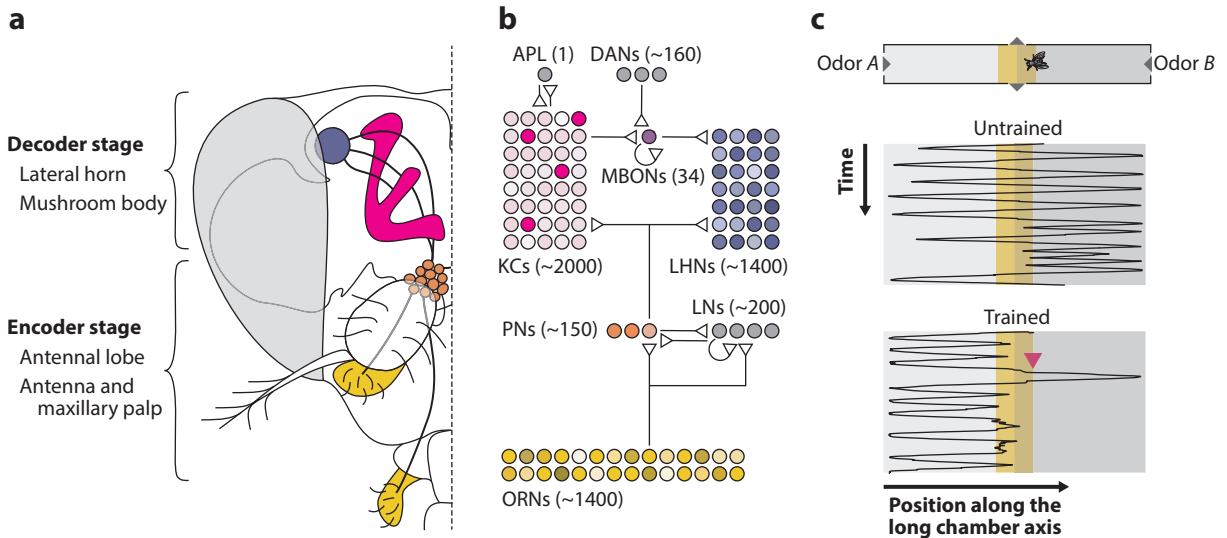


Figure 1

Odor discrimination. (*a, b*) The olfactory system of fruit flies at macroscopic (*a*) and circuit scales (*b*). The encoder stage comprises olfactory receptor neurons (ORNs, *yellow*), projection neurons (PNs, *orange*), and local neurons (LNs, *gray*) of the antennal lobe. The decoder stage consists of Kenyon cells (KCs, *pink*), mushroom body output neurons (MBONs, *purple*), and lateral horn neurons (LHNs, *blue*). The anterior paired lateral neuron (APL, *gray*) provides feedback inhibition to KCs. Synaptic strengths from KCs to MBONs are modulated by dopaminergic neurons (DANs, *gray*). Circles in panel *b* represent ~ 50 neurons; colors symbolize odor-evoked activity; numbers in parentheses indicate approximate neuron numbers per hemisphere. (*c*) Behavioral measurements. Odor stream *A* and odor stream *B* converge at the center of a narrow chamber (*top*). Odor discrimination is analyzed by tracking the position of a fly along the long chamber axis as a function of time. The fraction of choices in favor of odor *A* or odor *B* is an index of naive preference (*center*) or trained accuracy (*bottom*); the time elapsing between entry into and exit from the central decision zone (*yellow*) is quantified as the reaction time. The arrowhead in the bottom panel marks an incorrect choice.

these extremes. Binding of ligand stabilizes the receptor in its open or closed conformation (21) and accordingly increases or decreases the spike frequency of the cognate ORN from a variable background rate of 1–31 Hz, with an average of 8 Hz (31, 32, 54, 55). This spontaneous background activity arises from thermal fluctuations of the odorant receptors between their closed and open states and constitutes the main source of noise in the olfactory system (71). Exchanging receptors between ORN types transfers the odor selectivity, response polarity, transduction dynamics, and thermal breathing pattern of the donor's receptor to the recipient cell (33, 55).

Although ORNs expressing the same functional receptor gene appear scattered across the sensory surface, their axons establish a precise one-to-one correspondence with ~ 50 different types of excitatory projection neurons (PNs) in the antennal lobes (45, 70, 141) (**Figure 1a,b**). The centerpiece of each of these parallel communication channels is a morphologically identifiable synaptic relay, termed a glomerulus (130), where the bilaterally projecting axons of 20–200 ORNs are matched in an all-to-all fashion with the dendrites of an average of 3 strictly unilateral excitatory PNs (70, 75). All PNs innervating the same glomerulus thus receive input from at least a tenfold larger ORN population. Because the members of this population have identical receptive fields but spike independently of one another (75), input pooling improves the signal-to-noise ratio of PNs and allows them to detect small odor-evoked firing rate changes in a noisy barrage of spontaneous ORN activity (68). Reciprocal dendrodendritic connections between sister PNs innervating the same glomerulus enhance activity correlations further, perhaps to aid synchrony-based decoding downstream (68, 75).

PN: projection neuron

Glomerulus: compact cluster of synaptic connections between ORNs of one type and their cognate PNs

Adaptation

As the concentration of an odor rises, the number of active glomerular channels and the ORN firing rate modulation from baseline grow (54, 102, 131, 142). This odor-evoked activity quickly alters the sensitivity of the ORN through Ca^{2+} -mediated negative feedback that causes the dephosphorylation of the odorant receptor (53, 132): Epochs of strong excitation attenuate subsequent odor responses, whereas periods of inhibition boost them (31, 100). The consequences of this cell-autonomous adaptation are twofold.

First, ORNs can adjust their coding strategy to the statistics of their input signals and represent a wider range of stimuli than their available dynamic range of approximately two orders of magnitude in odor concentration would allow (49). The price of any adaptive code, however, is ambiguity: Because ORN responses adapt, they reflect not only the current olfactory environment but also its recent history. To resolve this ambiguity and discern odors irrespective of concentration (94), distinguish different intensities of the same odor (12, 29, 35, 94), or detect a salient cue in the presence of a high level of distractor (29), flies must encode this context. Motion-sensitive H1 neurons in the visual system solve an analogous problem by multiplexing instantaneous and contextual signals in the same spike train at different timescales (37). Whether olfaction has evolved a similar solution is unknown.

A second consequence of adaptation is that long presentations of an odor cause spike rates to peak and then decay to a plateau above baseline (7, 76, 100). In other words, ORNs are differential-proportional sensors whose activity maxima emphasize changes in odorant receptor occupancy. The pronounced short-term depression of ORN-to-PN synapses (74)—a property tied to their high release probability—further accentuates change relative to the steady state. The effects of these differentiating filters are evident also in the odor responses of second-order (7, 77) and third-order (51) olfactory neurons.

Combinatorial Odor Encoding

In the most simplistic view, a glomerular odor representation consists of a combination of inactive and active channels, written as an ordered list of ~ 50 zeros and ones. Counting the number of positions at which two lists differ yields a measure of their dissimilarity, the Hamming distance (56, 102). The average Hamming distance in an ensemble of binary code words of the same length is maximal—and the capacity of the corresponding code is therefore largest, or the task of discriminating a fixed number of messages in this code is easiest—if zeros and ones occur with equal probability. Depending on chemical identity and concentration, natural or naturalistic odor blends, as well as monomolecular odorants, elicit responses from 5% to 95% of all odorant receptors or glomerular channels; the mean response rates of 24 receptors and 16 glomeruli, averaged over some 130 odors and odor concentrations tested, range from 38% to 69% (54, 55, 102, 146) (**Figure 1b**). These empirical response rates are sufficiently close to the theoretical optimum of 50% to suggest that odor representations at the encoder stage of the olfactory system approach a state of maximum entropy (102, 128, 129).

A more realistic view of odor encoding will take into account not only the number of active channels but also the level of activity within them. Instead of a list of zeros and ones, a glomerular odor representation then becomes a vector with ~ 50 components (one for the spike frequency in each channel), and taxicab, Euclidean, and cosine distances replace Hamming distances as pairwise dissimilarity metrics (80, 110). The taxicab distance has an intuitive interpretation: It represents the summed activity differences in all channels. The Euclidean distance measures the length of the line segment connecting the tips of two activity vectors, whereas the cosine distance quantifies the angle between them; it ranges from a maximum of one when the vectors are orthogonal (indicating

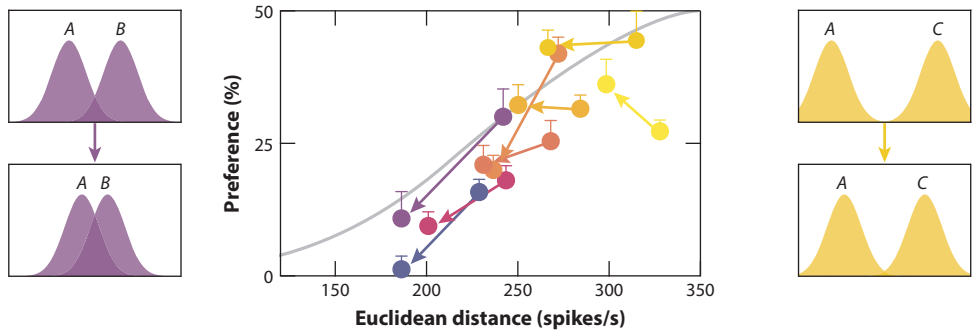


Figure 2

Reducing the separation between the stimulus–conditional neuronal response distributions of odors impairs their discriminability (schematics on the *left* and *right*). The central plot shows the naive preferences of flies discriminating two odors as a function of the Euclidean distances between the corresponding projection neuron activity vectors (means \pm SEM, $n = 30$ – 40 flies per data point). Colored arrows denote changes in Euclidean distance and preference caused by silencing transmission in four of the ~ 50 glomerular channels; the solid gray line indicates wild-type performance. The central panel was adapted from Reference 110. Abbreviation: spikes/s, spikes per second.

little overlap in neural activity) to a minimum of zero when the vectors are parallel (and the activity patterns are similar in structure but not necessarily in magnitude). Taxicab and Euclidean distances are therefore sensitive to overall activity levels, whereas cosine distances are not.

Activity differences provide a natural currency for the analysis of sensory discrimination. A typical behavioral experiment asks whether differences in odor-evoked activity are large enough to be perceived by an animal as it moves from one olfactory environment to another (**Figure 1c**). The experiment therefore does not probe the animal’s ability to pinpoint the exact identity and absolute concentration of an odor in a vast set of possible alternatives but poses a much simpler question: Judging from the neural activity patterns they elicit, are two odors the same, or are they different? In theory, this classical signal detection problem is solved by inspecting the stimulus–conditional response distributions (also known as the likelihood functions) and finding the activity threshold that achieves the best trade-off between discrimination failures and false alarms (50). Consider a hypothetical olfactory system with a single glomerular channel that responds strongly to odor *A*, more weakly to odor *B*, and barely to odor *C*. Because the means of the likelihood functions $P(R|A)$ and $P(R|C)$ are so widely separated, the brain can easily set a threshold that achieves accurate discrimination between odors *A* and *C* (**Figure 2**). The situation is different for odors *A* and *B*, whose discriminability is lower owing to their overlapping likelihood functions. Here, as in general, the decision rule generating the fewest overall errors is based on likelihood ratio (50): if, for a given activity level R in the glomerular channel, $P(R|A)/P(R|B) > 1$, decide *A*; otherwise, decide *B*. This flexible rule, whose criterion can be adjusted to accommodate unequal prior probabilities or unequal rewards or penalties for correct or incorrect responses (47, 123), produces a logistic (sigmoidal) psychometric function.

Logistic relationships between stimulus contrast and performance appear commonly in two-choice sensory discrimination tasks (13, 50, 97, 101, 116, 139). Their characteristic shape arises from a logit link between (a) physical stimulus attribute(s) and choice probability, consistent with the idea that the brain uses the weight of evidence or log likelihood ratio to decide (46, 48). Odor identity discrimination by flies is no exception: A logistic function of contrast in the glomerular transmission line places an upper bound on performance (110) (**Figure 2**). To estimate the contrast available to the decoders that read PN signals, the mean firing rates of the 24 ORN classes

Psychometric

function: fraction of correct decisions as a function of a stimulus attribute (e.g., contrast)

with empirically determined odor response spectra (54, 55) were computationally converted to the corresponding PN firing rates. The conversion took into account the effects of short-term depression of ORN-to-PN synapses (74) and the relative refractory period of PNs, which conspire to cap transmission rates, and a gain control mechanism at the level of the antennal lobes (see below) (106). Although the 24-dimensional PN activity vectors cover only a subspace of the ~ 50 -dimensional coding space, their distances predict the ability of flies to distinguish odor pairs (110), suggesting that the partial vectors are representative of the encoder as a whole. Flies show little or no behavioral bias when the distance between the representations of two odors is small, achieve saturating levels of bias when the distance is large, and tend to display intermediate bias in the transition region between plateaux. The inflection point of half-maximal discrimination is located at a taxicab distance of ~ 850 PN spikes per second (which extrapolates to an activity difference of $\sim 1,750$ PN spikes per second in all channels), a Euclidean distance of ~ 220 PN spikes per second (**Figure 2**), or a cosine distance of ~ 0.3 . These distances appear large, even against a background of $\sim 1,500$ PN spikes per second that arises from the bombardment of the antennal lobes by $\sim 20,000$ spontaneous ORN spikes per second (31, 32).

It is important to stress that the sizeable activity differences needed for innate odor discrimination reflect inefficient decoding of PN activity by the default decoder, the lateral horn of the protocerebrum (**Figure 1a,b**), rather than lossy encoding or transmission of sensory information: A different decoder, the mushroom body (**Figure 1a,b**), which is engaged after training (59), achieves much finer discrimination of odors from the very same PN spike trains. Trained flies have no difficulty discriminating the odor pair separated by the shortest distance among the 5,995 possible combinations of the 110 characterized monomolecular odorants (110), and experimental animals with only a single functional glomerular channel—the hypothetical situation we considered when discussing likelihood ratio—can be trained to pick up on inferred activity differences as small as 216 versus 234 PN spikes per second in that channel (30). Flies, like other species (42), likely exploit temporal structure in the odor-evoked activity to aid discrimination. For example, if the response to one odor peaked well before the other, the odors should be distinguishable in different temporal windows after stimulus onset.

Perhaps because innate odor discrimination is so relatively inefficient, it offers some of the clearest illustrations of how changing the separation between the means of the stimulus-conditional response distributions affects behavior. The complete masking of one odor by another—the holy grail of the air freshener industry—is a striking example. Contrasting an attractant with a powerful repellant, which would be expected to make the pleasant scent even more attractive, can in fact extinguish all behavioral bias if the neuronal response distributions of the two odors overlap broadly (110): If an animal cannot distinguish the odors, it cannot express a preference. Likewise, silencing circumscribed subsets of glomerular channels shrinks the distances between odor representations whose contrast hinges on activity in the manipulated channels (110). The behavioral consequences of this intervention depend on the margin of safety in the original separation of the response distributions (**Figure 2**): If the separation is large, the distributions can be moved closer without creating overlap and compromising discrimination; if the initial separation is marginal, reducing it further causes performance to slide (110).

As appealing as likelihood ratio is as a decision rule, its neural implementation poses a significant hurdle (46). In our example of a single glomerular channel that responds strongly to odor *A* and more weakly to odor *B* (**Figure 2**), the system would need to know the full likelihood functions $P(R|A)$ and $P(R|B)$ and the manner in which these functions change dynamically (7, 42, 49, 76, 77, 100), for instance, as a result of receptor adaptation (53, 132), to decide between *A* and *B* from a single observation *R*. The hurdle can be overcome by introducing a second population of neurons whose odor responses are the exact opposite of the first; these “antineurons”

LN: local interneuron of the antennal lobe

GABA:
 γ -aminobutyric acid

LHN: lateral horn neuron

(13, 101) thus respond strongly to odor *B* and more weakly to odor *A*. The activity difference in the two channels is then equivalent to log likelihood ratio (46, 47). While it is difficult to imagine precisely mirror-symmetric neuron–antineuron pairs for all odor combinations that a fly could possibly encounter, comparisons of activity in differently tuned channels are of course implicit in distance-based discrimination (110). However, whether this computation can also approximate a log likelihood ratio test has not been formally explored. In situations where only differences in odor intensity need to be discerned, cells that fit the strict neuron–antineuron bill rather closely (by responding antagonistically to increases or decreases in concentration) are found at several stages of the olfactory system (21, 51, 65, 95).

Gain Control and High-Pass Filtering

Odorant receptor adaptation and the compressive nonlinearity of ORN-to-PN synapses, which amplifies weak ORN inputs, attenuates strong inputs, and thereby equalizes response magnitudes across the PN population (90, 99, 106), are the first in a line of buffers that regulate the gain and offset of the encoder.

Each antennal lobe contains a population of at least ~ 100 ipsilaterally and ~ 100 bilaterally projecting local neurons (LNs) (24) (**Figure 1b**). Most LNs are inhibitory and release γ -aminobutyric acid (GABA) (103, 145); a minority are cholinergic (24, 125); some secrete (a) currently unidentified transmitter(s) (24); and many form gap junctions (63, 148). In contrast with the stereotyped anatomy of ORNs and PNs in the backbone of the glomerular relay (27, 40, 45, 70, 130, 141), LNs display an unusual degree of morphological and functional variation. An analysis of 1,489 ipsilaterally projecting LNs revealed 847 distinct morphologies (24), many more than the number of neurons per lobe. Most flies' LN complements must therefore differ from one another. Collectively, however, this motley crew of inhibitory LNs seems to perform the same, invariant task of covering all glomeruli in a near-uniform blanket of feedback inhibition. The magnitude of this feedback scales with total ORN activity (106), and its principal targets are the ORN axon terminals themselves (107, 117). Although there is room for added complexities—dendritic release of acetylcholine by PNs (102) may also drive LN activity (146) (**Figure 1b**), PN dendrites (145, 148) and fellow LNs (63, 145, 148) may also be targets of inhibition (**Figure 1b**), LN output may be spatially structured (102), and the sensitivity to GABA may differ among glomeruli (117)—their functional impact seems minor, at least in the context of the rate-code representations of odors we consider here: Global, uniform, exclusively ORN-driven lateral inhibition alone predicts PN from ORN firing rates with high accuracy (106). The overall effect of this so-called divisive normalization or input gain control (106) is to decorrelate PN channels and stretch the cosine (but not the Euclidean) distances between the means of the stimulus–conditional response distributions (**Figure 3a,b**). Increased separation, of course, facilitates discrimination.

A remarkably similar gain control mechanism also operates on the axon terminals of PNs in the lateral horn but involves feedforward instead of feedback inhibition (110). The source of inhibition is a group of ~ 40 GABAergic PNs with multiglomerular dendrites whose axons bypass the mushroom bodies (70, 103). Once again, inhibition scales with total ORN activity and acts presynaptically, in a manner that suppresses transmission at low, but not at high, firing rates (110). A chief difference between this high-pass filter and gain control in the antennal lobe is the number of glomerular channels that the postsynaptic neuron samples. PNs of one glomerulus are driven by a single ORN class (45, 70, 141), and gain control regulates their sensitivity to this dominant excitatory input. Lateral horn neurons (LHNs), in contrast, connect to an average of six glomeruli (67), and the high-pass filter eliminates weakly active elements from the corresponding input vectors (110). The result is a decorrelation of synaptic input patterns, as is evident from the sizeable increase in cosine distances (110) (**Figure 3c,d**).

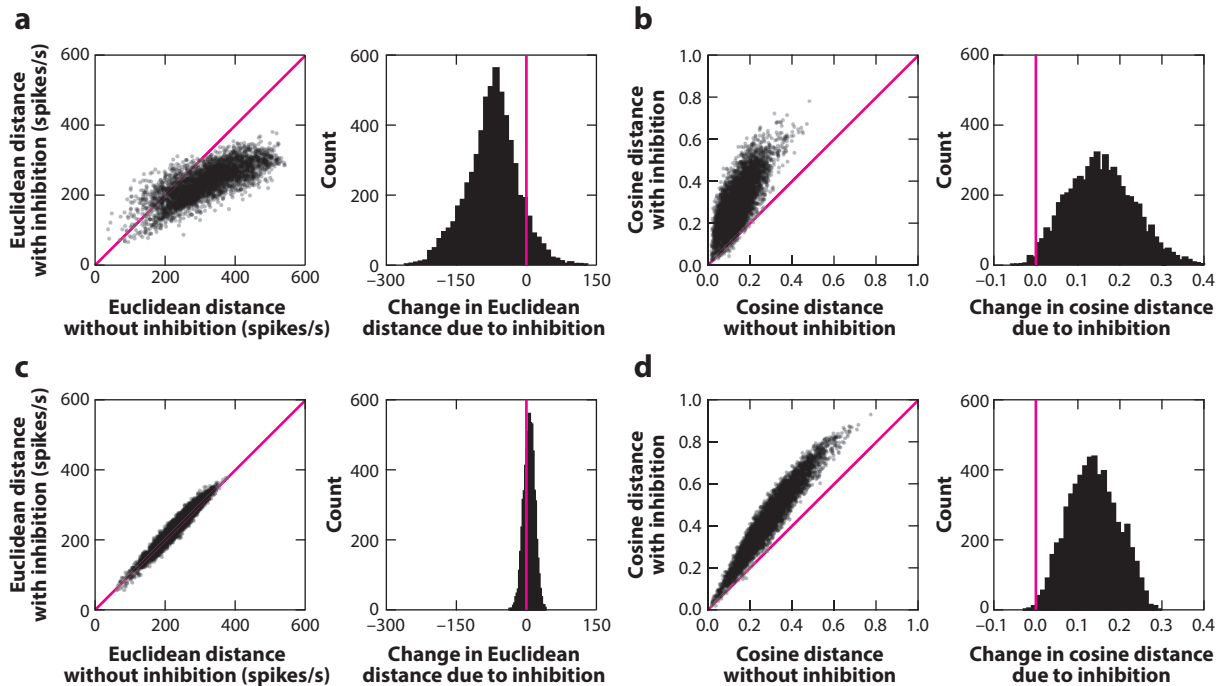


Figure 3

Effects of inhibitory gain control at olfactory receptor neuron (ORN) terminals (*a* and *b*) and inhibitory high-pass filtering at projection neuron (PN) terminals (*c* and *d*) on Euclidean (*a* and *c*) and cosine distances (*b* and *d*) between PN activity vectors. Scatter plots compare the 5,995 possible pairwise distances between 110 odors in the presence and absence of inhibition; histograms quantify net distance changes due to inhibition. Panels *c* and *d* were adapted from Reference 110. Abbreviation: spikes/s, spikes per second.

Stochastic Resonance

All gain control mechanisms described so far are active at high stimulus intensities and involve negative feedback at the cellular and circuit levels. The gain of sensory transduction is feedback controlled (31, 100), and transmission by ORN and PN terminals is inhibited at high stimulus strengths (106, 107, 110, 117). By contrast, very little is known about positive gain control mechanisms that enhance neuronal responses to low-intensity stimuli. Threshold detectors, such as LHNs or the Kenyon cells (KCs) of the mushroom bodies, are by their very nature blind to sub-threshold inputs but could, in principle, be sensitized to such signals by adding a nonspecific—even noisy—offset that lifts weak activity above threshold. This simple mechanism, which is known under the somewhat misleading moniker of “stochastic resonance,” is an inevitable property of nonlinear devices that perform thresholding operations on their inputs (43).

The antennal lobe contains neurons and connections that seem suited to provide this nonspecific positive offset. A small, broadly odor-responsive population of LNs synthesize and secrete acetylcholine, the predominant excitatory transmitter in the fly brain, diffusely in all glomeruli; its release can depolarize PNs (63, 125). In addition, the same population of LNs (and perhaps also others) are gap junction-coupled to PNs (63, 148). The existence of lateral, electrical and chemical, excitatory connections explains persistent PN responses after the experimental elimination of all direct ORN input (105, 118, 125). Owing to the prohibitive difficulty of targeting these connections cleanly and comprehensively for experimental manipulations, however, the idea that

KC: Kenyon cell

lateral excitation amplifies low-intensity signals to make them detectable to downstream decoders remains untested.

MBON: mushroom body output neuron

DAN: dopaminergic input neuron to the mushroom body

THE DECODER STAGE

Two Systems

The bifurcating axons of PNs project combinatorial odor images onto two discrete decoders: the lateral protocerebra and the mushroom bodies (66, 70, 92, 130, 147) (**Figure 1a,b**). The roles of these structures in odor discrimination bring to mind Kahneman's Systems 1 and 2 (72). The lateral horn resembles System 1: fast, stereotyped, and coarse, an autopilot for innate behaviors. The mushroom body is reminiscent of System 2: slower, experience-based, and finely discriminating.

System 1, the lateral horn, contains at least 1,410 neurons per hemisphere (41). Five hundred and eighty locally projecting and 830 distantly projecting LHNs fall into anywhere between 39 and 150 distinct types on the basis of anatomical, genetic, and functional criteria (41, 67). LHNs, therefore, are a somewhat smaller but more variegated population than KCs, the intrinsic neurons of the mushroom bodies (see below). Individual LHNs sample from up to 21 different PN afferents (67), which target the lateral horn in a broadly stereotypical manner (39, 69, 92, 147). Certain glomerular combinations are overrepresented, both within and between LHN types, perhaps because the corresponding chemical mixtures define ethologically important "odor scenes" (67). In addition to these combinatorial feature detectors, dedicated hotlines exist for monomolecular salients: PNs of the DA1 glomerulus, for example, respond to the pheromone 11-*cis*-vaccenyl acetate (82) and project, quite possibly as the sole input to one type of LHN, to a circumscribed and sexually dimorphic region of the lateral protocerebrum (69, 78, 119).

System 2, the mushroom body, operates in a side loop between the antennal lobe and the lateral horn (34, 66) (**Figure 1a,b**) and is essential for learned (59) but dispensable for innate odor discrimination (110). Olfactory information continuously flows through the mushroom body loop, but the positive and negative valences assigned to it in the untrained ground state are in such perfect equipoise that their effects on behavior cancel (108). Learning creates an imbalance that is expressed as a behavioral bias and can be mimicked—without training—by switching on or off mushroom body output neurons (MBONs) contributing to the net zero balance of positive and negative valence signals in the ground state (108).

The internal architecture of the mushroom body, like that of the cerebellum, features all necessary elements of a random-access memory (25, 73). About 2,000 mushroom body-intrinsic KCs per hemisphere (2) serve as address decoders by drawing random—to a first approximation (150)—samples of 2–11 inputs from the ~50 glomerular address lines (22, 98) with postsynaptic claws that wrap around a corresponding number of PN terminals (85). All KC axons initially gather in a tight bundle, the peduncle, which subsequently splits into vertical and horizontal lobes; the axonal projection patterns of KCs into these lobes define seven genetically (137) and also, where electrophysiological data exist, biophysically distinct neuronal classes (51, 64, 138). Although the functional significance of this subdivision remains—with a few exceptions (29, 79)—mysterious, the common treatment of the KC ensemble as a homogeneous population is undoubtedly an oversimplification.

Dendritic integration of PN inputs determines whether a memory address is activated for reading or writing; the efferent KC synapses constitute the actual data storage locations (60, 104, 108, 122). About 50–100 of these cholinergic synapses (5, 136) are arranged, like pearls on a string, along each axonal fiber as it intersects the arborizations of MBONs and their cognate dopaminergic neurons (DANs) (**Figure 1b**), which serve as read and write lines, respectively (25, 73). Twenty-one types of MBONs and their DAN companions (25, 91) define 16 memory compartments that

tile the mushroom body lobes (2, 136); MBONs directing attraction and aversion, and DANs providing negative and positive reinforcement (16, 25, 89), are segregated along the vertical and horizontal axes (3). Because active KC-to-MBON synapses depress when exposed to dopamine (60, 104, 122), pairing MBONs and DANs in a sign-reversed arrangement—MBONs directing attraction with aversively reinforcing DANs and vice versa (2, 3)—ensures that negative reinforcement weakens the positive value associated with an odor, whereas positive reinforcement does the opposite. Intercompartmental inhibition (2) contributes in some cases to the self-cancellation of MBON output in the untrained state (111).

The addressing system employs three strategies to maximize odor discrimination: Expansion recoding and sparse connectivity between PNs and KCs segregate the means of the stimulus-conditional response distributions in a high-dimensional coding space; feedback inhibition compresses the distributions' variances; and sequential sampling allows the contrast between representations to grow over time.

Expansion Recoding and Sparsening

Early theoretical work on the cerebellum proposed that expansion recoding (projecting activity onto a large number of neurons) and sparsening (reducing the fraction of active neurons) would promote stimulus separation (1, 93). In the mushroom body, the expansion ratio from ~ 150 PNs to $\sim 2,000$ KCs is ~ 13.3 on purely anatomical grounds but increases to ~ 40 if the functional redundancy among sister PNs (75) is taken into account. The expansion ratio from cerebellar mossy fibers to granule cells is similar (88).

The number of unique KC addresses would peak if each KC randomly drew (with replacement) ~ 25 presynaptic partners from the ~ 50 glomerular channels, but the combinatorial explosion of possible wiring patterns allows many fewer synapses to generate adequate diversity. In fact, keeping connections relatively sparse avoids correlations that would counteract the benefit of a large synaptic degree (23, 88). If the number of synapses is fixed, for either wiring or energetic reasons, there is therefore an optimal degree of connectivity at which the discriminability of all stimulus-conditional response distributions is maximal. This optimum depends on the distribution of synaptic weights, which adds variability to postsynaptic currents, and on the presence of inhibitory feedback, which expands the decoder's dynamic range by permitting KC thresholds to vary with stimulus strength (88). For a mushroom body with ~ 50 glomerular address lines, a total of 14,000 afferent synapses, an empirically determined synaptic weight distribution (51), and the single anterior paired lateral neuron providing global feedback inhibition (see below), the optimal figures are 2,000 KCs with an average of 7 excitatory inputs each (88). These figures agree closely with the actual number of KCs and the average claw count per cell (22, 85, 88).

The 50-choose-7 input connectivity of KCs can produce nearly 10 million unique 7-digit addresses, far more than the actual number of neurons per mushroom body. Each KC may therefore connect to a unique combination of glomeruli, as was indeed seen in a fully mapped sample of 200 cells (22). The population sparseness of KC responses to odors, however, is smaller than this diversity of wiring patterns would superficially suggest: An average of 5–10% of all KCs respond to any given odor (62, 87, 138). This moderate level of sparseness likely arises from three sources: First, PNs represent odors in a format approximating a maximum entropy code, so odors are expected to activate half of the digits of any address (102, 128, 129). Second, not all digits that make up an address need to be coactive to drive spiking; depending on the synaptic input strengths and the KC's intrinsic excitability, activity in one to four of the average seven excitatory inputs may suffice (52). Third, *Drosophila* KCs can summate synaptic inputs over time; they are therefore not pure coincidence detectors (51, 52).

APL: anterior paired lateral neuron

Drift-diffusion model:

a phenomenological model of decision making as the accumulation of noisy evidence to a threshold

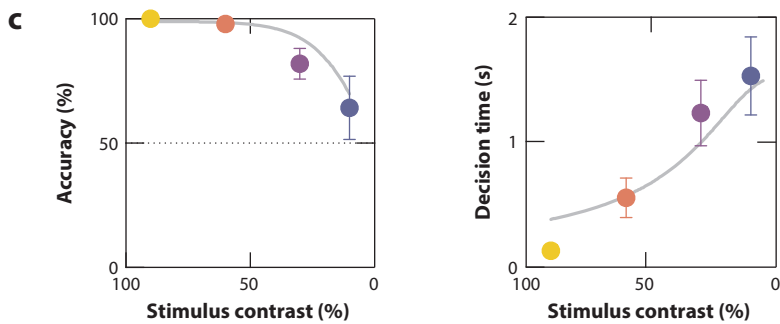
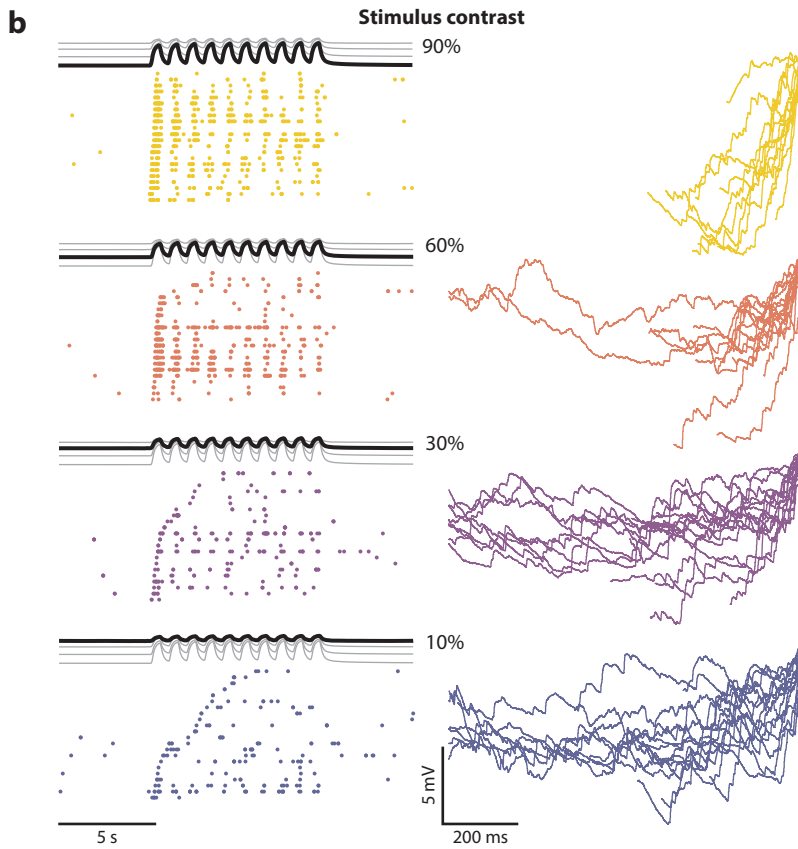
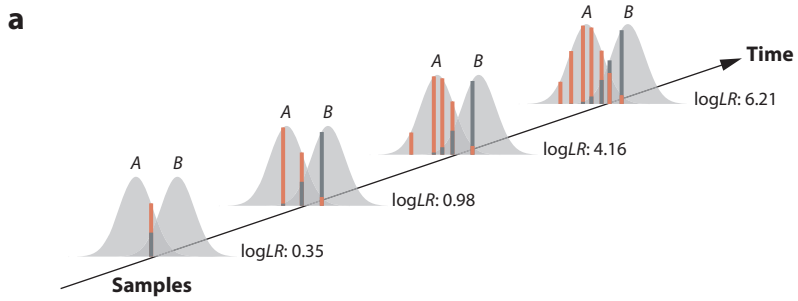
The observed level of population sparseness must in fact be enforced by the giant GABAergic anterior paired lateral neuron (APL) (87, 109), which exists in a single copy per hemisphere (**Figure 1b**) (137). APL imposes a variable threshold on the overall activity across the decoder stage that silences all but the top 5–10% of KCs and thus keeps the variances of the response distributions in check. APL is activated by and provides global inhibition to the entire KC population (87), with some variation among KC divisions (64). Disrupting this inhibitory feedback loop widens the odor tuning of KCs, as reflected in increasingly correlated and broadly distributed somatic calcium signals (87). This effect is paralleled by changes in learned olfactory choice behavior that, again, depend on the initial degree of separation of the response distributions: Dissimilar odor pairs remain discernible, whereas similar odors blur into one another (87).

Because population sparseness is moderate, parallel odor representations may exist in most of or all the seven KC divisions. Under the assumption that sparseness is similar for all KC classes [which is almost certainly incorrect (51), but which we make for the sake of the present argument], even the smallest division, $\alpha'\beta'_m$ (137), is expected to respond to odors with activity in ~ 10 of its ~ 140 members. An intriguing hypothesis (128) posits that the randomness of their afferent connections allows KCs to form a sparsifying basis in which odors can be represented especially concisely. A dozen or so of these “compressed sensors” (20) would then suffice to recover all the information encoded in the ~ 50 glomerular channels (128). Functional imaging experiments lend some credence to this idea: Calcium signals recorded from a group of 12–50 randomly selected KCs predict, with reasonable accuracy, the animals’ learned odor preference (19).

Sequential Sampling

While judgments based on single samples of ambiguous evidence tend to be unreliable, combining information from multiple observations over time can gradually tease apart even broadly overlapping stimulus–conditional response distributions (**Figure 4a**). The corresponding statistical framework—sequential analysis—has its origin in quality control and cryptanalysis, where data are evaluated as they are collected until a stopping criterion is met (10, 47, 48, 50). The stopping criterion forms an absorbing boundary to which the accumulating evidence advances in a biased random walk (or, in the continuous limit, a diffusion process with drift): Each new piece of information moves the accumulated total closer toward or away from the boundary (10, 47, 113, 123). The stronger the sensory evidence, the more powerful the biasing force, and the fewer samples are needed before the process stops. For the binary decisions that are typically studied in the laboratory and which concern us here, either a single decision variable moving between two bounds (one for each option) quantifies the relative evidence favoring one alternative over the other, or two separate accumulators racing against each other gather absolute evidence for each of the competing options (10, 47, 123). If the two alternatives have equal prior probability and the two accumulators are anticorrelated, the difference between these so-called symmetric random walk and race models is so subtle that it becomes negligible for our purposes (10, 47, 123). The models do, however, differ in how easily they lend themselves to a biophysical interpretation: Race models find a natural correspondence in the evaluation of log likelihood ratio by neuron–antineuron pairs (46, 123).

When flies discriminate two odors (or, more accurately, two concentrations of one odor), the membrane potentials of KCs in the $\alpha\beta_c$ division of the mushroom bodies drift noisily toward action potential threshold (51), just as a continuously updated tally of absolute evidence would drift toward a decision bound (**Figure 4b**). Two separate groups of $\alpha\beta_c$ KCs, termed up and down cells, respond to increases or decreases in odor concentration and can therefore assume the roles of neurons and antineurons (13, 101) in a race between two integrators (51). A voltage gap of



(Caption appears on following page)

Figure 4 (Figure appears on preceding page)

Sequential sampling. (a) The log likelihood ratio ($\log LR$) favoring odor *A* over odor *B* increases with the number of samples. (b) Examples of spike rasters (left) and membrane voltages preceding the first $\alpha\beta_c$ Kenyon cell (KC) spike (right) in response to odor concentration changes at low (blue), intermediate (purple and orange), and high contrast (yellow). The spike rasters are sorted, in ascending order from the bottom, by the latency of the first spike after stimulus onset. The membrane potential traces are aligned to the upstroke of the action potential and depict a period of ≤ 1 second. (c) Accuracy (left) and speed (right) of odor intensity discrimination as functions of stimulus contrast. Solid gray lines depict drift-diffusion fits to behavioral accuracy and decision time measurements (1,245 flies and 4,910 decisions, respectively); colored circles denote neurometric estimates based on the timing and fidelity of the first $\alpha\beta_c$ KC spikes after odor concentration changes at low (blue), intermediate (purple and orange), and high contrast (yellow) (means \pm SEM, $n = 36$ –66 trials from 7 to 13 cells per data point). Panels *b* and *c* were adapted from Reference 51.

~ 8 mV—much wider than that of other KC types—separates the resting potentials and spike thresholds of $\alpha\beta_c$ KCs and suppresses virtually all spontaneous activity. Closing this voltage gap requires a minimum of six or seven perfectly coincident PN inputs; in reality, excitatory postsynaptic potentials (EPSPs) arrive nonsynchronously and must be summed over time (51). The extremely thin, elongated dendrites of $\alpha\beta_c$ KCs (149) act as temporal filters that slow the decay of EPSPs and provide accumulator memory. A critical influence on the persistence of this memory is the dendritic voltage-gated A-type potassium channel *Shal* (K_{V4}) (143), which regulates the amplitude, time course, and propagation of EPSPs (18, 51, 61). Because *Shal* currents oppose synaptically evoked voltage changes (18, 51, 61), the number of EPSPs needed to fire an $\alpha\beta_c$ KC action potential exceeds the theoretical minimum of half a dozen by a factor depending on the strength of the sensory evidence: High-contrast stimuli (that is, large odor concentration changes) drive high-frequency transmission from PNs, which results in steep, rapid KC depolarizations to spike threshold, whereas low-contrast stimuli cause a trickle of synaptic release, shallow, meandering membrane potential changes, and long spike latencies (51) (Figure 4b). A particular constellation of biophysical properties thus allows $\alpha\beta_c$ KCs to perform sequential analysis on their synaptic inputs, using the discharge of an action potential as the stopping rule.

The conclusion that $\alpha\beta_c$ KCs encode accumulating evidence in subliminal voltage changes rests on four pillars of experimental support. First, neurometric functions based on the timing of the first $\alpha\beta_c$ KC spike account for the behavior of the decision-making animal (51) (Figure 4c). Second, psychophysical measurements of speed and accuracy yield an estimate of diffusion noise in the decision process (29). Electrophysiological measurements of the membrane potential noise of $\alpha\beta_c$ KCs match this estimate (51). Third, the membrane density of *Shal* in $\alpha\beta_c$ KCs is kept within narrow limits by the forkhead box P (*FoxP*) transcription factor (51). Mutating *FoxP* derepresses the *Shal* promoter, augments A-type currents, hastens the decay of EPSPs, and prolongs spike latencies. Mutating *FoxP* also prolongs decision times—to the same extent that it prolongs spike latencies (29, 51). Fourth, the biophysical and behavioral defects of *FoxP* mutants can be repaired by blocking *Shal*, and they can be introduced into wild-type flies by overexpressing *Shal* exclusively in $\alpha\beta_c$ KCs (51).

The ability to alter decision times by changing a single ionic current in a small, well-defined population of neurons (51) sets these analyses apart from studies of perceptual decisions in other systems. Much thinking about neural mechanisms of sequential sampling has revolved around spike-based phenomena, such as smooth, ramp-like increases in firing rate (57, 116, 124), discrete jumps from low to high activity (which can create the appearance of ramping if jumps occur stochastically in a population) (84), or the progression of activity toward choice-specific attractors (58). Is subthreshold integration by $\alpha\beta_c$ KCs therefore an idiosyncrasy? Perhaps not—a recent spate of perceptual studies in the mouse highlights at least some commonalities. Mice can

EPSP: excitatory postsynaptic potential

Neurometric function: probability that an ideal observer could infer a stimulus attribute (e.g., contrast) from a neuronal response

perform a simple visual discrimination task even when the relevant neurons in the primary visual cortex are allowed to emit, at most, a single spike (114); the necessary computations must be completed in the interval containing (or preceding) that spike. Like the latencies of $\alpha\beta_c$ KCs, the spike latencies of neurons in the piriform cortex increase with decreasing odor intensity contrast while their average firing rates remain virtually constant; accordingly, spike times report odor concentration more reliably than absolute spike rates do (11). And, glutamatergic neurons in the periaqueductal gray (PAG) impose a synaptic threshold on excitatory inputs from the superior colliculus that encode looming threat; the first PAG spikes trigger escape in accordance with a drift-diffusion model of threat integration (36). In contrast with $\alpha\beta_c$ KCs, however, which implement both the integration process and the stopping rule (51), PAG neurons merely threshold a signal that is integrated presynaptically, by recurrently connected collicular neurons whose efferent synapses facilitate as activity builds up (36).

At first sight, the role of Shal in $\alpha\beta_c$ KCs is puzzling: What would be the advantage of an imperfect integrator that leaks information during collection? We speculate that there may be an optimal half-life to evidence: too short, and temporal integration will fail outright; too long, and even noise will eventually add up to commitment. Put slightly differently, the time constant of the accumulator's memory should be matched to the expected arrival rate of sensory evidence. The details of this match then determine the stringency of the decision criterion and the degree to which behavioral choices are insulated from random fluctuations in sensory input. Because Shal activates at depolarized voltages (143), evidence acquired recently (and, therefore, close to spike threshold) is discounted more heavily than evidence collected further in the past, when the cell remained near resting potential and the channel's open probability was negligible (51). This effect could partially counteract the inevitable fading of earlier samples with time and enable approximately linear integration.

Neuronal Noise and Behavioral Variability

Behavior is irreducibly variable: Even when confronted with clear-cut evidence, animals make the occasional odd (or exploratory) choice. Flies discriminating two odors, for example, display a maximal accuracy of no more than $\sim 98\%$ (29). The random walk (or diffusion) component of the drift-diffusion framework captures this unpredictability formally but is agnostic about its biophysical origin. *Drosophila FoxP* mutants now point to a potential source of behavioral variability: Despite their prolonged reaction times, these mutants discriminate odors with the same accuracy as wild-type flies (29). This dissociation of accuracy from speed was initially thought to reflect a compensatory elevation of the decision bound, which would offset the reduced drift rate and, therefore, the larger relative contribution of diffusion noise (29). Intracellular recordings subsequently proved this conjecture incorrect: The decision bounds—that is, the spike thresholds—of wild-type and FoxP-deficient $\alpha\beta_c$ KCs are identical (51). Instead, the abundance of Shal in *FoxP* mutants reduces the sensory-evoked drift in membrane voltage to the same extent as it reduces membrane potential noise, maintaining a constant ratio (51). This tight covariation of signal and noise suggests a common sensory origin for both and implies that $\alpha\beta_c$ KCs are virtually noiseless accumulators, echoing a similar inference drawn from psychophysical and modeling studies in humans and rats (15). Behavioral variability may thus have its roots in noisy sensory evidence or an intrinsically noisy encoder stage and not in the capriciousness of System 2.

DISCLOSURE STATEMENT

The authors are not aware of any affiliations, memberships, funding, or financial holdings that might be perceived as affecting the objectivity of this review.

ACKNOWLEDGMENTS

We thank Moshe Parnas for help with **Figure 3** and Shamik DasGupta for comments. Work in the authors' laboratory is supported by the Wellcome Trust and the Gatsby Charitable Foundation.

LITERATURE CITED

1. Albus JS. 1971. A theory of cerebellar function. *Math. Biosci.* 10:25–61
2. Aso Y, Hattori D, Yu Y, Johnston RM, Iyer NA, et al. 2014. The neuronal architecture of the mushroom body provides a logic for associative learning. *eLife* 3:e04577
3. Aso Y, Sitaraman D, Ichinose T, Kaun KR, Vogt K, et al. 2014. Mushroom body output neurons encode valence and guide memory-based action selection in *Drosophila*. *eLife* 4:e04580
4. Barlow HB. 1961. Possible principles underlying the transformation of sensory messages. In *Sensory Communication*, ed. WA Rosenblith, pp. 217–34. Cambridge, MA: MIT Press
5. Barnstedt O, Oswald D, Felsenberg J, Brain R, Moszynski J-P, et al. 2016. Memory-relevant mushroom body output synapses are cholinergic. *Neuron* 89:1237–47
6. Benton R, Vannice KS, Gomez-Diaz C, Vosshall LB. 2009. Variant ionotropic glutamate receptors as chemosensory receptors in *Drosophila*. *Cell* 136:149–62
7. Bhandawat V, Olsen SR, Gouwens NW, Schlieff ML, Wilson RI. 2007. Sensory processing in the *Drosophila* antennal lobe increases reliability and separability of ensemble odor representations. *Nat. Neurosci.* 10:1474–82
8. Bialek W. 2012. *Biophysics: Searching for Principles*. Princeton, NJ: Princeton Univ. Press
9. Bialek W, Rieke F, de Ruyter van Steveninck RR, Warland D. 1991. Reading a neural code. *Science* 252:1854–57
10. Bogacz R, Brown E, Moehlis J, Holmes P, Cohen JD. 2006. The physics of optimal decision making: a formal analysis of models of performance in two-alternative forced-choice tasks. *Psychol. Rev.* 113:700–65
11. Bolding KA, Franks KM. 2017. Complementary codes for odor identity and intensity in olfactory cortex. *eLife* 6:e22630
12. Borst A. 1983. Computation of olfactory signals in *Drosophila melanogaster*. *J. Comp. Physiol. A* 152:373–83
13. Britten KH, Shadlen MN, Newsome WT, Movshon JA. 1992. The analysis of visual motion: a comparison of neuronal and psychophysical performance. *J. Neurosci.* 12:4745–65
14. Brunet LJ, Gold GH, Ngai J. 1996. General anosmia caused by a targeted disruption of the mouse olfactory cyclic nucleotide-gated cation channel. *Neuron* 17:681–93
15. Brunton BW, Botvinick MM, Brody CD. 2013. Rats and humans can optimally accumulate evidence for decision-making. *Science* 340:95–98
16. Burke CJ, Huetteroth W, Oswald D, Perisse E, Krashes MJ, et al. 2012. Layered reward signalling through octopamine and dopamine in *Drosophila*. *Nature* 492:433–37
17. Butterwick JA, del Marmol J, Kim KH, Kahlson MA, Rogow JA, et al. 2018. Cryo-EM structure of the insect olfactory receptor Orco. *Nature* 560:447–52
18. Cai X, Liang CW, Muralidharan S, Kao JPY, Tang C-M, et al. 2004. Unique roles of SK and Kv4.2 potassium channels in dendritic integration. *Neuron* 44:351–64
19. Campbell RAA, Honegger KS, Qin H, Li W, Demir E, Turner GC. 2013. Imaging a population code for odor identity in the *Drosophila* mushroom body. *J. Neurosci.* 33:10568–81
20. Candès EJ, Wakin MB. 2008. An introduction to compressive sampling: a sensing/sampling paradigm that goes against the common knowledge in data acquisition. *IEEE Signal Process. Mag.* 25:21–30
21. Cao L-H, Yang D, Wu W, Zeng X, Jing B-Y, et al. 2017. Odor-evoked inhibition of olfactory sensory neurons drives olfactory perception in *Drosophila*. *Nat. Commun.* 8:1357
22. Caron SJC, Ruta V, Abbott LF, Axel R. 2013. Random convergence of olfactory inputs in the *Drosophila* mushroom body. *Nature* 497:113–17
23. Cayco-Gajic NA, Clopath C, Silver RA. 2017. Sparse synaptic connectivity is required for decorrelation and pattern separation in feedforward networks. *Nat. Commun.* 8:1116
24. Chou Y-H, Spletter ML, Yaksi E, Leong JCS, Wilson RI, Luo L. 2010. Diversity and wiring variability of olfactory local interneurons in the *Drosophila* antennal lobe. *Nat. Neurosci.* 13:439–49

25. Claridge-Chang A, Roorda RD, Vrontou E, Sjulson L, Li H, et al. 2009. Writing memories with light-addressable reinforcement circuitry. *Cell* 139:405–15
26. Clyne PJ, Warr CG, Freeman MR, Lessing D, Kim J, Carlson JR. 1999. A novel family of divergent seven-transmembrane proteins: candidate odorant receptors in *Drosophila*. *Neuron* 22:327–38
27. Couto A, Alenius M, Dickson BJ. 2005. Molecular, anatomical, and functional organization of the *Drosophila* olfactory system. *Curr. Biol.* 15:1535–47
28. Cover TM, Thomas JA. 1991. *Elements of Information Theory*. New York: Wiley
29. DasGupta S, Ferreira CH, Miesenböck G. 2014. FoxP influences the speed and accuracy of a perceptual decision in *Drosophila*. *Science* 344:901–4
30. DasGupta S, Waddell S. 2008. Learned odor discrimination in *Drosophila* without combinatorial odor maps in the antennal lobe. *Curr. Biol.* 18:1668–74
31. de Bruyne M, Clyne PJ, Carlson JR. 1999. Odor coding in a model olfactory organ: the *Drosophila* maxillary palp. *J. Neurosci.* 19:4520–32
32. de Bruyne M, Foster K, Carlson JR. 2001. Odor coding in the *Drosophila* antenna. *Neuron* 30:537–52
33. Dobritsa AA, van der Goes van Naters W, Warr CG, Steinbrecht RA, Carlson JR. 2003. Integrating the molecular and cellular basis of odor coding in the *Drosophila* antenna. *Neuron* 37:827–41
34. Dolan M-J, Belliart-Guérin G, Bates AS, Frechter S, Lampin-Saint-Amaux A, et al. 2018. Communication from learned to innate olfactory processing centers is required for memory retrieval in *Drosophila*. *Neuron* 100:651–68
35. Dudai Y. 1977. Properties of learning and memory in *Drosophila melanogaster*. *J. Comp. Physiol. A* 114:69–89
36. Evans DA, Stempel AV, Vale R, Ruehle S, Lefler Y, Branco T. 2018. A synaptic threshold mechanism for computing escape decisions. *Nature* 558:90–94
37. Fairhall AL, Lewen GD, Bialek W, de Ruyter van Steveninck RR. 2001. Efficiency and ambiguity in an adaptive neural code. *Nature* 412:787–92
38. Farris SM. 2011. Are mushroom bodies cerebellum-like structures? *Arthropod Struct. Dev.* 40:368–79
39. Fişek M, Wilson RI. 2014. Stereotyped connectivity and computations in higher-order olfactory neurons. *Nat. Neurosci.* 17:280–88
40. Fishilevich E, Vosshall LB. 2005. Genetic and functional subdivision of the *Drosophila* antennal lobe. *Curr. Biol.* 15:1548–53
41. Frechter S, Bates AS, Tootoonian S, Dolan M-J, Manton JD, et al. 2018. Functional and anatomical specificity in a higher olfactory centre. bioRxiv 336982. <https://doi.org/10.1101/336982>
42. Friedrich RW, Laurent G. 2001. Dynamic optimization of odor representations by slow temporal patterning of mitral cell activity. *Science* 291:889–94
43. Gammaitoni L, Hänggi P, Jung P, Marchesoni F. 1998. Stochastic resonance. *Rev. Mod. Phys.* 70:223–87
44. Gao Q, Chess A. 1999. Identification of candidate *Drosophila* olfactory receptors from genomic DNA sequence. *Genomics* 60:31–39
45. Gao Q, Yuan B, Chess A. 2000. Convergent projections of *Drosophila* olfactory neurons to specific glomeruli in the antennal lobe. *Nat. Neurosci.* 3:780–85
46. Gold JI, Shadlen MN. 2001. Neural computations that underlie decisions about sensory stimuli. *Trends Cogn. Sci.* 5:10–16
47. Gold JI, Shadlen MN. 2007. The neural basis of decision making. *Annu. Rev. Neurosci.* 30:535–74
48. Good IJ. 1985. Weight of evidence: a brief survey. In *Bayesian Statistics 2*, ed. JM Bernardo, MH DeGroot, DV Lindley, AFM Smith, pp. 249–69. Amsterdam: Elsevier Sci.
49. Gorur-Shandilya S, Demir M, Long J, Clark DA, Emonet T. 2017. Olfactory receptor neurons use gain control and complementary kinetics to encode intermittent odorant stimuli. *eLife* 6:e27670
50. Green DM, Swets JA. 1966. *Signal Detection Theory and Psychophysics*. New York: Wiley
51. Groschner LN, Chan Wah Hak L, Bogacz R, DasGupta S, Miesenböck G. 2018. Dendritic integration of sensory evidence in perceptual decision-making. *Cell* 173:894–905.e13
52. Gruntman E, Turner GC. 2013. Integration of the olfactory code across dendritic claws of single mushroom body neurons. *Nat. Neurosci.* 16:1821–29

53. Guo H, Kunwar K, Smith D. 2017. Odorant receptor sensitivity modulation in *Drosophila*. *J. Neurosci.* 37:9465–73
54. Hallem EA, Carlson JR. 2006. Coding of odors by a receptor repertoire. *Cell* 125:143–60
55. Hallem EA, Ho MG, Carlson JR. 2004. The molecular basis of odor coding in the *Drosophila* antenna. *Cell* 117:965–79
56. Hamming RW. 1980. *Coding and Information Theory*. Englewood Cliffs, NJ: Prentice-Hall
57. Hanes DP, Schall JD. 1996. Neural control of voluntary movement initiation. *Science* 274:427–30
58. Harvey CD, Coen P, Tank DW. 2012. Choice-specific sequences in parietal cortex during a virtual-navigation decision task. *Nature* 484:62–68
59. Heisenberg M, Borst A, Wagner S, Byers D. 1985. *Drosophila* mushroom body mutants are deficient in olfactory learning. *J. Neurogenet.* 2:1–30
60. Hige T, Aso Y, Modi MN, Rubin GM, Turner GC. 2015. Heterosynaptic plasticity underlies aversive olfactory learning in *Drosophila*. *Neuron* 88:985–98
61. Hoffman DA, Magee JC, Colbert CM, Johnston D. 1997. K⁺ channel regulation of signal propagation in dendrites of hippocampal pyramidal neurons. *Nature* 387:869–75
62. Honegger KS, Campbell RAA, Turner GC. 2011. Cellular-resolution population imaging reveals robust sparse coding in the *Drosophila* mushroom body. *J. Neurosci.* 31:11772–85
63. Huang J, Zhang W, Qiao W, Hu A, Wang Z. 2010. Functional connectivity and selective odor responses of excitatory local interneurons in *Drosophila* antennal lobe. *Neuron* 67:1021–33
64. Inada K, Tsuchimoto Y, Kazama H. 2017. Origins of cell-type-specific olfactory processing in the *Drosophila* mushroom body circuit. *Neuron* 95:357–67.e4
65. Ito I, Ong RC-Y, Raman B, Stopfer M. 2008. Sparse odor representation and olfactory learning. *Nat. Neurosci.* 11:1177–84
66. Ito K, Suzuki K, Estes P, Ramaswami M, Yamamoto D, Stausfeld NJ. 1998. The organization of extrinsic neurons and their implications in the functional roles of the mushroom bodies in the *Drosophila melanogaster* Meigen. *Learn. Mem.* 5:52–77
67. Jeanne JM, Fişek M, Wilson RI. 2018. The organization of projections from olfactory glomeruli onto higher-order neurons. *Neuron* 98:1198–213.e6
68. Jeanne JM, Wilson RI. 2015. Convergence, divergence, and reconvergence in a feedforward network improves neural speed and accuracy. *Neuron* 88:1014–26
69. Jefferis GS, Potter CJ, Chan AM, Marin EC, Rohlfling T, et al. 2007. Comprehensive maps of *Drosophila* higher olfactory centers: spatially segregated fruit and pheromone representation. *Cell* 128:1187–203
70. Jefferis GSXE, Marin E, Stocker RF, Luo L. 2001. Target neuron prespecification in the olfactory map of *Drosophila*. *Nature* 414:204–8
71. Joseph J, Dunn FA, Stopfer M. 2012. Spontaneous olfactory receptor neuron activity determines follower cell response properties. *J. Neurosci.* 32:2900–10
72. Kahneman D. 2011. *Thinking, Fast and Slow*. New York: Farrar, Strous and Giroux
73. Kanerva P. 1988. *Sparse Distributed Memory*. Cambridge, MA: MIT Press
74. Kazama H, Wilson RI. 2008. Homeostatic matching and nonlinear amplification at identified central synapses. *Neuron* 58:401–13
75. Kazama H, Wilson RI. 2009. Origins of correlated activity in an olfactory circuit. *Nat. Neurosci.* 12:1136–44
76. Kim AJ, Lazar AA, Slutskiy YB. 2011. System identification of *Drosophila* olfactory sensory neurons. *J. Comput. Neurosci.* 30:143–61
77. Kim AJ, Lazar AA, Slutskiy YB. 2015. Projection neurons in *Drosophila* antennal lobes signal the acceleration of odor concentrations. *eLife* 4:e06651
78. Kohl J, Ostrovsky AD, Frechter S, Jefferis GSXE. 2013. A bidirectional circuit switch reroutes pheromone signals in male and female brains. *Cell* 155:1610–23
79. Krashes MJ, Keene AC, Leung B, Armstrong JD, Waddell S. 2007. Sequential use of mushroom body neuron subsets during *Drosophila* odor memory processing. *Neuron* 53:103–15
80. Kreher SA, Mathew D, Kim J, Carlson JR. 2008. Translation of sensory input into behavioral output via an olfactory system. *Neuron* 59:110–24

81. Kullback S. 1959. *Information Theory and Statistics*. New York: Wiley
82. Kurtovic A, Widmer A, Dickson BJ. 2007. A single class of olfactory neurons mediates behavioural responses to a *Drosophila* sex pheromone. *Nature* 446:542–46
83. Larsson MC, Domingos AI, Jones WD, Chiappe ME, Amrein H, Vosshall LB. 2004. Or83b encodes a broadly expressed odorant receptor essential for *Drosophila* olfaction. *Neuron* 43:703–14
84. Latimer KW, Yates JL, Meister MLR, Huk AC, Pillow JW. 2015. Single-trial spike trains in parietal cortex reveal discrete steps during decision-making. *Science* 349:184–87
85. Leiss F, Groh C, Butcher NJ, Meinertzhagen IA, Tavosanis G. 2009. Synaptic organization in the adult *Drosophila* mushroom body calyx. *J. Comp. Neurol.* 517:808–24
86. Lima SQ, Miesenböck G. 2005. Remote control of behavior through genetically targeted photostimulation of neurons. *Cell* 121:141–52
87. Lin AC, Bygrave AM, de Calignon A, Lee T, Miesenböck G. 2014. Sparse, decorrelated odor coding in the mushroom body enhances learned odor discrimination. *Nat. Neurosci.* 17:559–68
88. Litwin-Kumar A, Harris KD, Axel R, Sompolinsky H, Abbott LF. 2017. Optimal degrees of synaptic connectivity. *Neuron* 93:1153–57
89. Liu C, Plaçais P-Y, Yamagata N, Pfeiffer BD, Aso Y, et al. 2012. A subset of dopamine neurons signals reward for odour memory in *Drosophila*. *Nature* 488:512–16
90. Luo SX, Axel R, Abbott LF. 2010. Generating sparse and selective third-order responses in the olfactory system of the fly. *PNAS* 107:10713–18
91. Mao Z, Davis RL. 2009. Eight different types of dopaminergic neurons innervate the *Drosophila* mushroom body neuropil: anatomical and physiological heterogeneity. *Front. Neural Circuits* 3:5
92. Marin EC, Jefferis GSXE, Komiyama T, Zhu H, Luo L. 2002. Representation of the glomerular olfactory map in the *Drosophila* brain. *Cell* 109:243–55
93. Marr D. 1969. A theory of cerebellar cortex. *J. Physiol.* 202:437–70
94. Masek P, Heisenberg M. 2008. Distinct memories of odor intensity and quality in *Drosophila*. *PNAS* 105:15985–90
95. Mazor O, Laurent G. 2005. Transient dynamics versus fixed points in odor representations by locust antennal lobe projection neurons. *Neuron* 48:661–73
96. Miesenböck G. 2009. The optogenetic catechism. *Science* 326:395–99
97. Mountcastle VB, Steinmetz MA, Romo R. 1990. Frequency discrimination in the sense of flutter: psychophysical measurements correlated with postcentral events in behaving monkeys. *J. Neurosci.* 10:3032–44
98. Murthy M, Fiete I, Laurent G. 2008. Testing odor response stereotypy in the *Drosophila* mushroom body. *Neuron* 59:1009–23
99. Nagel KI, Hong EJ, Wilson RI. 2015. Synaptic and circuit mechanisms promoting broadband transmission of olfactory stimulus dynamics. *Nat. Neurosci.* 18:56–65
100. Nagel KI, Wilson RI. 2011. Biophysical mechanisms underlying olfactory receptor neuron dynamics. *Nat. Neurosci.* 14:208–16
101. Newsome WT, Britten KH, Movshon JA. 1989. Neuronal correlates of a perceptual decision. *Nature* 341:52–54
102. Ng M, Roorda RD, Lima SQ, Zemelman BV, Morcillo P, Miesenböck G. 2002. Transmission of olfactory information between three populations of neurons in the antennal lobe of the fly. *Neuron* 36:463–74
103. Okada R, Awasaki T, Ito K. 2009. Gamma-aminobutyric acid (GABA)-mediated neural connections in the *Drosophila* antennal lobe. *J. Comp. Neurol.* 514:74–91
104. Okada R, Rybak J, Manz G, Menzel R. 2007. Learning-related plasticity in PE1 and other mushroom body-extrinsic neurons in the honeybee brain. *J. Neurosci.* 27:11736–47
105. Olsen SR, Bhandawat V, Wilson RI. 2007. Excitatory interactions between olfactory processing channels in the *Drosophila* antennal lobe. *Neuron* 54:89–103
106. Olsen SR, Bhandawat V, Wilson RI. 2010. Divisive normalization in olfactory population codes. *Neuron* 66:287–99
107. Olsen SR, Wilson RI. 2008. Lateral presynaptic inhibition mediates gain control in an olfactory circuit. *Nature* 452:956–60

108. Oswald D, Felsenberg J, Tallbot CB, Das G, Perisse E, et al. 2015. Activity of defined mushroom body output neurons underlies learned olfactory behavior in *Drosophila*. *Neuron* 86:417–27
109. Papadopoulou M, Cassenaer S, Nowotny T, Laurent G. 2011. Normalization for sparse encoding of odors by a wide-field interneuron. *Science* 332:721–25
110. Parnas M, Lin AC, Huetteroth W, Miesenböck G. 2013. Odor discrimination in *Drosophila*: from neural population codes to behavior. *Neuron* 79:932–44
111. Perisse E, Oswald D, Barnstedt O, Tallbot CB, Huetteroth W, Waddell S. 2016. Aversive learning and appetitive motivation toggle feed-forward inhibition in the *Drosophila* mushroom body. *Neuron* 90:1086–99
112. Pikielny CW, Hasan G, Rouyer F, Rosbash M. 1994. Members of a family of *Drosophila* putative odorant-binding proteins are expressed in different subsets of olfactory hairs. *Neuron* 12:35–49
113. Ratcliff R. 1978. Theory of memory retrieval. *Psychol. Rev.* 85:59–108
114. Resulaj A, Ruediger S, Olsen SR, Scanziani M. 2018. First spikes in visual cortex enable perceptual discrimination. *eLife* 7:e34044
115. Rieke F, Warland D, de Ruyter van Steveninck R, Bialek W. 1997. *Spikes: Exploring the Neural Code*. Cambridge, MA: MIT Press
116. Roitman JD, Shadlen MN. 2002. Response of neurons in the lateral intraparietal area during a combined visual discrimination reaction time task. *J. Neurosci.* 22:9475–89
117. Root CM, Masuyama K, Green DS, Enell LE, Nässel DR, et al. 2008. A presynaptic gain control mechanism fine-tunes olfactory behavior. *Neuron* 59:311–21
118. Root CM, Semmelhack JL, Wong AM, Flores J, Wang JW. 2007. Propagation of olfactory information in *Drosophila*. *PNAS* 104:11826–31
119. Ruta V, Datta SR, Vasconcelos ML, Freeland J, Looger LL, Axel R. 2010. A dimorphic pheromone circuit in *Drosophila* from sensory input to descending output. *Nature* 468:686–90
120. Sato K, Pellegrino M, Nakagawa T, Nakagawa T, Vosshall LB, Touhara K. 2008. Insect olfactory receptors are heteromeric ligand-gated ion channels. *Nature* 452:1002–6
121. Schuckel J, Törkkel PH, French AS. 2009. Two interacting olfactory transduction mechanisms have linked polarities and dynamics in *Drosophila melanogaster* antennal basiconic sensilla neurons. *J. Neurophysiol.* 102:214–23
122. Séjourné J, Plaçais P-Y, Aso Y, Siwanowicz I, Trannoy S, et al. 2011. Mushroom body efferent neurons responsible for aversive olfactory memory retrieval in *Drosophila*. *Nat. Neurosci.* 14:903–10
123. Shadlen MN, Kiani R. 2013. Decision making as a window on cognition. *Neuron* 80:791–806
124. Shadlen MN, Newsome WT. 2001. Neural basis of a perceptual decision in the parietal cortex (area LIP) of the rhesus monkey. *J. Neurophysiol.* 86:1916–36
125. Shang Y, Claridge-Chang A, Sjulson L, Pypaert M, Miesenböck G. 2007. Excitatory local circuits and their implications for olfactory processing in the fly antennal lobe. *Cell* 128:601–12
126. Shlens J. 2014. Notes on Kullback-Leibler divergence and likelihood. arXiv 1404.2000[cs.IT]
127. Simoncelli EP, Olshausen BA. 2001. Natural image statistics and neural representation. *Annu. Rev. Neurosci.* 24:1193–216
128. Stevens CF. 2015. What the fly's nose tells the fly's brain. *PNAS* 112:9460–65
129. Stevens CF. 2016. A statistical property of fly odor responses is conserved across odors. *PNAS* 113:6737–42
130. Stocker RF. 1994. The organization of the chemosensory system in *Drosophila melanogaster*: a review. *Cell Tissue Res.* 275:3–26
131. Stopfer M, Jayaraman V, Laurent G. 2003. Intensity versus identity coding in an olfactory system. *Neuron* 39:991–1004
132. Störtkuhl KF, Hovemann BT, Carlson JR. 1999. Olfactory adaptation depends on the Trp Ca²⁺ channel in *Drosophila*. *J. Neurosci.* 19:4839–46
133. Strausfeld NJ, Hansen L, Li Y, Gomez RS, Ito K. 1998. Evolution, discovery, and interpretations of arthropod mushroom bodies. *Learn Mem.* 5:11–37
134. Suh GS, Wong AM, Hergarden AC, Wang JW, Simon AF, et al. 2004. A single population of olfactory sensory neurons mediates an innate avoidance behaviour in *Drosophila*. *Nature* 431:854–59

135. Szyszka P, Gerkin RC, Galizia CG, Smith BH. 2014. High-speed odor transduction and pulse tracking by insect olfactory receptor neurons. *PNAS* 111:16925–30
136. Takemura S-Y, Aso Y, Hige T, Wong A, Lu Z, et al. 2017. A connectome of a learning and memory center in the adult *Drosophila* brain. *eLife* 6:e26975
137. Tanaka NK, Tanimoto H, Ito K. 2008. Neuronal assemblies of the *Drosophila* mushroom body. *J. Comp. Neurol.* 508:711–55
138. Turner GC, Bazhenov M, Laurent G. 2008. Olfactory representations by *Drosophila* mushroom body neurons. *J. Neurophysiol.* 99:734–46
139. Uchida N, Mainen ZF. 2003. Speed and accuracy of olfactory discrimination in the rat. *Nat. Neurosci.* 6:1224–29
140. Vosshall LB, Amrein H, Morozov PS, Rzhetsky A, Axel R. 1999. A spatial map of olfactory receptor expression in the *Drosophila* antenna. *Cell* 96:725–36
141. Vosshall LB, Wong AM, Axel R. 2000. An olfactory sensory map in the fly brain. *Cell* 102:147–59
142. Wang JW, Wong AM, Flores J, Vosshall LB, Axel R. 2003. Two-photon calcium imaging reveals an odor-evoked map of activity in the fly brain. *Cell* 112:271–82
143. Wei A, Covarrubias M, Butler A, Baker K, Pak M, Salkoff L. 1990. K⁺ current diversity is produced by an extended gene family conserved in *Drosophila* and mouse. *Science* 248:599–603
144. Wicher D, Schäfer R, Bauernfeind R, Stensmyr MC, Heller R, et al. 2008. *Drosophila* odorant receptors are both ligand-gated and cyclic-nucleotide-activated cation channels. *Nature* 452:1007–11
145. Wilson RI, Laurent G. 2005. Role of GABAergic inhibition in shaping odor-evoked spatiotemporal patterns in the *Drosophila* antennal lobe. *J. Neurosci.* 25:9069–79
146. Wilson RI, Turner GC, Laurent G. 2004. Transformation of olfactory representations in the *Drosophila* antennal lobe. *Science* 303:366–70
147. Wong AM, Wang JW, Axel R. 2002. Spatial representation of the glomerular map in the *Drosophila* protocerebrum. *Cell* 109:229–41
148. Yaksi E, Wilson RI. 2010. Electrical coupling between olfactory glomeruli. *Neuron* 67:1034–47
149. Yasuyama K, Meinertzhagen IA, Schürmann FW. 2002. Synaptic organization of the mushroom body calyx in *Drosophila melanogaster*. *J. Comp. Neurol.* 445:211–26
150. Zheng Z, Lauritzen JS, Perlman E, Robinson CG, Nichols M, et al. 2018. A complete electron microscopy volume of the brain of adult *Drosophila melanogaster*. *Cell* 174:730–43.e22